

# Role of the $\text{H}_2^+$ channel in the primordial star formation under strong radiation field and the critical intensity for the supermassive star formation

K. Sugimura,<sup>1\*</sup> C. M. Coppola,<sup>2,3</sup> K. Omukai,<sup>1</sup> D. Galli<sup>3</sup> and F. Palla<sup>3</sup>

<sup>1</sup>*Astronomical Institute, Tohoku University, Aoba, Sendai 980-8578, Japan*

<sup>2</sup>*Dipartimento di Chimica, Università degli Studi di Bari, Via Orabona 4, I-70126 Bari, Italy*

<sup>3</sup>*INAF-Osservatorio Astrofisico di Arcetri, Largo E. Fermi 5, I-50125 Firenze, Italy*

24 September 2018

## ABSTRACT

We investigate the role of the  $\text{H}_2^+$  channel on  $\text{H}_2$  molecule formation during the collapse of primordial gas clouds immersed in strong radiation fields which are assumed to have the shape of a diluted black-body spectra with temperature  $T_{\text{rad}}$ . Since the photodissociation rate of  $\text{H}_2^+$  depends on its level population, we take full account of the vibrationally-resolved  $\text{H}_2^+$  kinetics. We find that in clouds under soft but intense radiation fields with spectral temperature  $T_{\text{rad}} \lesssim 7000$  K, the  $\text{H}_2^+$  channel is the dominant  $\text{H}_2$  formation process. On the other hand, for harder spectra with  $T_{\text{rad}} \gtrsim 7000$  K, the  $\text{H}^-$  channel takes over  $\text{H}_2^+$  in the production of molecular hydrogen. We calculate the critical radiation intensity needed for supermassive star formation by direct collapse and examine its dependence on the  $\text{H}_2^+$  level population. Under the assumption of local thermodynamic equilibrium (LTE) level population, the critical intensity is underestimated by a factor of a few for soft spectra with  $T_{\text{rad}} \lesssim 7000$  K. For harder spectra, the value of the critical intensity is not affected by the level population of  $\text{H}_2^+$ . This result justifies previous estimates of the critical intensity assuming LTE populations since radiation sources like young and/or metal-poor galaxies are predicted to have rather hard spectra.

**Key words:** quasars: supermassive black holes-molecular processes-cosmology: theory.

## 1 INTRODUCTION

The collapse of primordial gas clouds can lead to the formation of ordinarily-massive stars ( $10 - 100 M_{\odot}$ , hereafter Pop III stars; see, e.g., Yoshida et al. 2008; Hosokawa et al. 2011) or supermassive stars ( $M \gtrsim 10^5 M_{\odot}$ , hereafter SMS; see, e.g., Bromm & Loeb 2003), depending on the strength of the radiation fields in the ambient medium. Pop III stars form by  $\text{H}_2$  cooling in the absence of a strong Lyman-Werner (LW) radiation field ( $h\nu = 11.2 - 13.6$  eV). Conversely, in a cloud irradiated by an extremely strong LW radiation field,  $\text{H}_2$  is completely destroyed, and cooling is suppressed. In the latter case, if the cloud is in a halo with virial temperature higher than  $\sim 10^4$  K, it can still collapse via atomic cooling (Omukai 2001), without experiencing major episodes of fragmentation (Bromm & Loeb 2003; Regan & Haehnelt 2009a,b; Inayoshi et al. 2014; Latif et al. 2014; Regan et al. 2014a,b; Choi et al. 2015; Becerra et al. 2015), and an em-

bryonic protostar can grow rapidly to a SMS by subsequent accretion (Hosokawa et al. 2012, 2013; Sakurai et al. 2015; Shlosman et al. 2015). The latter eventually collapses due to the post-Newtonian instability, leaving a black hole with  $\sim 10^5 M_{\odot}$  (see, e.g., Shapiro & Teukolsky 1983). This process, called “direct”, or “monolithic” collapse, leads to the formation of SMS remnants that are promising candidates for being the seeds of the supermassive ( $\gtrsim 10^9 M_{\odot}$ ) black holes (SMBHs) observed at redshift  $z \gtrsim 6$  (see, e.g., Fan et al. 2001; Mortlock et al. 2011; Venemans et al. 2013; Wu et al. 2015)).

The feasibility of this scenario can be tested by comparing the observed number density of the high- $z$  SMBHs  $n_{\text{SMBH}}$  with the theoretical predictions. By considering the probability distribution of the LW intensity  $J_{21}$  around halos<sup>1</sup>,  $n_{\text{SMBH}}$  can be estimated from the critical value of LW intensity  $J_{21}^{\text{crit}}$  needed for the formation of SMS (Dijkstra

\* E-mail: sugimura@astr.tohoku.ac.jp

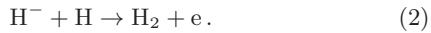
<sup>1</sup> We use the specific intensity at the center of the LW bands,

et al. 2008; Agarwal et al. 2012; Dijkstra et al. 2014; Inayoshi & Tanaka 2015). Sugimura et al. (2014) (hereafter SOI14) found  $J_{21}^{\text{cr}} \sim 1000$  for realistic young-galaxy spectra. Combined with the  $J_{21}$  probability distribution by Dijkstra et al. (2014), this gives  $n_{\text{SMBH}} \sim 10^{-10} \text{ Mpc}^{-3}$ , in rough agreement with the observed values. However, the predicted  $n_{\text{SMBH}}$  is still uncertain due to our poor knowledge of  $J_{21}^{\text{cr}}$  from insufficient modelling of the physical/chemical processes in primordial gas clouds (see, e.g., Glover 2015a,b), and of the nature of the high-redshift sources responsible for this radiation.

In the low-density primordial gas ( $\lesssim 10^8 \text{ cm}^{-3}$ ),  $\text{H}_2$ , the main coolant in the low temperatures regime, is formed either via the  $\text{H}^-$  channel or via the  $\text{H}_2^+$  channel. The former begins with the formation of  $\text{H}^-$  by radiative attachment,



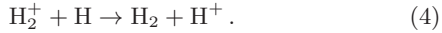
followed by  $\text{H}_2$  formation by associative detachment



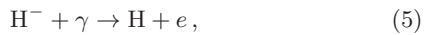
Similarly, the  $\text{H}_2^+$  channel starts with  $\text{H}_2^+$  formation by radiative association



followed by the charge transfer reaction



In each channel, the second step proceeds much faster than the first one and its rate determines the amount of  $\text{H}_2$  formation. Since the rate coefficient for reaction (1) ( $k_{\text{ra}}^{\text{H}^-} \sim 6 \times 10^{-15} \text{ cm}^3 \text{ s}^{-1}$  at 8000 K; Galli & Palla 1998, hereafter GP98) is about one order of magnitude larger than that for reaction (3) ( $k_{\text{ra}}^{\text{H}_2^+} \sim 1.5 \times 10^{-16} \text{ cm}^3 \text{ s}^{-1}$  at 8000 K; GP98), the  $\text{H}^-$  channel is usually much more efficient than that involving  $\text{H}_2^+$ . However, under a strong radiation field, both channels become irrelevant due to the destruction of the intermediaries by the  $\text{H}^-$  photodetachment



and  $\text{H}_2^+$  photodissociation



Since the binding energy of  $\text{H}^-$  (0.76 eV) is smaller than that of  $\text{H}_2^+$  (2.7 eV for the ground state),  $\text{H}^-$  is photodestroyed more easily than  $\text{H}_2^+$  and reaction (4) can become the dominant source of  $\text{H}_2$  in the primordial gas.

Here, it should be noted that the  $\text{H}_2^+$  photodissociation rate depends sensitively on the internal level population, because  $\text{H}_2^+$  in high vibrational levels is much more vulnerable to photodissociation. As an example, the binding energy of  $\text{H}_2^+$  in vibrational levels  $v = 6$  and 18 is only 1.2 and 0.003 eV, respectively. Thus, the level population of  $\text{H}_2^+$  is determined by a complex interplay of reactions, involving formation (reaction 3), collisional dissociation (reaction 4), photodissociation (reaction 6), collisional excitation/de-excitation and radiative de-excitation. Therefore in order to accurately implement the effects of the

$J_{21} \equiv J_{\nu}(h\nu = 12.4 \text{ eV})/10^{-21} \text{ erg s}^{-1} \text{ cm}^{-2} \text{ Hz}^{-1} \text{ sr}^{-1}$  to quantify the intensity of external radiation.

$\text{H}_2^+$  channel, a detailed calculation of its level population is needed.

In the post-recombination era,  $\text{H}_2$  formation is primarily controlled by the  $\text{H}_2^+$  channel for redshift  $z > 100$ , owing to the suppression of  $\text{H}^-$  by the cosmic microwave background (CMB) radiation (see, e.g., GP98). However, the efficiency of the  $\text{H}_2^+$  channel depends strongly on its level population: if  $\text{H}_2^+$  is in the ground state, the  $\text{H}_2^+$  channel is so efficient as to produce most of the  $\text{H}_2$  molecules at a level  $f_{\text{H}_2} \sim 10^{-4}$ . On the other hand, under local thermodynamic equilibrium (LTE), the  $\text{H}_2^+$  channel makes only a minor contribution to  $\text{H}_2$ , whose final abundance remains limited to  $f_{\text{H}_2} \sim 10^{-6}$ . Recently, Hirata & Padmanabhan (2006), Copola et al. (2011) (hereafter C11) and Longo et al. (2011) have studied the chemistry of the early Universe computing the population of the vibrational levels of  $\text{H}_2$  and  $\text{H}_2^+$  following a state-to-state reaction kinetics, and found that  $\text{H}_2^+$  forms by reaction (3) preferentially in excited states. As a result,  $\text{H}_2^+$  channel does not dominate the formation of  $\text{H}_2$ , and the final  $\text{H}_2$  abundance is limited by  $\text{H}^-$  at a level  $f_{\text{H}_2} \sim 10^{-6}$ .

Although the efficiency of the  $\text{H}_2^+$  channel depends strongly on the  $\text{H}_2^+$  level population, the LTE rate (Stancil 1994; Mihajlov et al. 2007) has been widely used in studying primordial gas clouds without a real justification. An exception is Glover (2015a) who calculated  $J_{21}^{\text{cr}}$  for black-body-type spectra with temperatures  $T_{\text{rad}} = 10^4 \text{ K}$  and  $10^5 \text{ K}$  under two assumptions for the  $\text{H}_2^+$  level population: (i) all the  $\text{H}_2^+$  is in the vibrational ground state, and (ii) all levels are in LTE. Although the difference in  $J_{21}^{\text{cr}}$  in the two cases is not significant, it is not yet clear in what circumstances and to what extent the  $\text{H}_2^+$  channel can affect the evolution of primordial gas clouds.

In this paper, we compute the thermal and chemical evolution of primordial gas clouds under a strong external radiation field with  $J_{21}$  around  $J_{21}^{\text{cr}}$  by computing the  $\text{H}_2^+$  vibrational level population, and assess the effect of  $\text{H}_2$  formation via the  $\text{H}_2^+$  channel. We also determine the critical intensity for supermassive star formation and examine its dependence on the  $\text{H}_2^+$  level population by comparing our non-LTE results to those obtained in the LTE or ground state approximations.

The paper is organized as follows. In Sec. 2, we describe our model for collapsing primordial gas clouds. In Sec. 3, we present the result of our calculation. The implications and conclusions are described Sec. 4.

## 2 MODEL

### 2.1 Basic Equations

To follow the gravitational collapse of primordial gas clouds, we use the one-zone model described in SOI14 (see also Omukai 2001), updated as follows: the vibrational level population of  $\text{H}_2^+$  is resolved following C11; a part of the chemical network is updated following Glover (2015a,b). In our model, we compute physical quantities in the homogeneous central part of the self-similar solution of collapsing clouds (Penston 1969; Larson 1969; Yahil 1983). The qualitative validity of the one-zone model has been confirmed recently by three-dimensional hydrodynamical simulations

(Shang et al. 2010; Latif et al. 2014). Thanks to the substantial simplification of gas dynamics, we can focus on the thermo-chemical processes in detail.

According to the one-zone model, the evolution of the gas density  $\rho$  is modeled as

$$\frac{d\rho}{dt} = \frac{\rho}{t_{\text{ff}}}, \quad (7)$$

where  $t_{\text{ff}} = \sqrt{3\pi/32G(\rho + \rho_{\text{DM}})}$  is the free-fall time,  $G$  the gravitational constant and  $\rho_{\text{DM}}$  the dark matter density, which is assumed to evolve following the solution of the spherical top-hat collapse model until it reaches the virial density. The radius of the core is approximately given by the Jeans length  $\lambda_{\text{J}} = \sqrt{\pi k T_{\text{gas}}/G\rho\mu m_{\text{p}}}$ , where  $m_{\text{p}}$  is the proton mass,  $\mu$  the mean molecular weight and  $k$  the Boltzmann constant. The evolution of the gas temperature  $T_{\text{gas}}$  is determined by the energy equation,

$$\frac{de_{\text{kin}}}{dt} = \Gamma_{\text{c}} - \Lambda_{\text{rad}} - \frac{de_{\text{int}}}{dt}, \quad (8)$$

where  $e_{\text{kin}} = 3kT_{\text{gas}}/2\mu m_{\text{p}}$  is the kinetic energy of the gas per unit mass,  $\Gamma_{\text{c}} = (\rho k T_{\text{gas}}/\mu m_{\text{p}})(d/dt)(1/\rho)$  the compressional heating rate,  $\Lambda_{\text{rad}}$  the net cooling/heating rate due to radiative processes and  $e_{\text{int}}$  the internal energy of the gas per unit mass, including both chemical energy and internal molecular energy. In the density and temperature range of our interest, the dominant cooling processes are  $\text{H}_2$  (Glover & Abel 2008), updated according to Glover (2015a), and Ly- $\alpha$  emission (Anninos et al. 1997). Other radiative reactions or the time variation of  $e_{\text{int}}$  hardly affect the evolution of  $T_{\text{gas}}$ .

We model the external radiation field as a diluted black-body with cut-off energy at 13.6 eV, specifying its temperature  $T_{\text{rad}}$  and intensity  $J_{21}$  at 12.4 eV. We limit our analysis to black-body spectra with various  $T_{\text{rad}}$  although realistic spectra of galaxies are more complex and not well represented by a black-body spectrum (SOI14, Agarwal & Khochfar 2015). SOI14 claimed that the ratio of the  $\text{H}^-$  photodetachment rate to the  $\text{H}_2$  photodissociation rate,  $k_{\text{pd}}^{\text{H}^-}/k_{\text{pd}}^{\text{H}_2}$ , is a key parameter characterizing the hardness of the spectra, and that typical young and/or metal-poor galaxies have hard spectra with  $k_{\text{pd}}^{\text{H}^-}/k_{\text{pd}}^{\text{H}_2} \lesssim 10^3$ , corresponding to black-body spectra with  $T_{\text{rad}} \gtrsim 2 \times 10^4$  K. Nonetheless, we explore a broad range of black-body temperatures,  $T_{\text{rad}} > 5 \times 10^3$  K, to mimic the evolution in a variety of environments possibly present in the early Universe.

## 2.2 Chemistry

In this section, we review our vibrationally-resolved chemical network based on SOI14 and C11. We consider 29 chemical species ( $\text{H}$ ,  $\text{H}^+$ ,  $\text{H}^-$ ,  $\text{H}_2$ ,  $\text{H}_2^+(v)$  with  $v = 0, 1 \dots, 18$ ,  $\text{He}$ ,  $\text{He}^+$ ,  $\text{He}^{2+}$ ,  $\text{HeH}^+$ ,  $\text{H}_3^+$  and  $\text{e}$ ), and we compute the evolution of the fractional abundance of species  $i$ ,  $y(i) \equiv n(i)/n_{\text{H}}$ , where  $n(i)$  is the number density of species  $i$  and  $n_{\text{H}}$  the number density of hydrogen nuclei. We do not consider deuterium chemistry because it should only affect the evolution of the gas with  $T_{\text{gas}}$  below a few hundred kelvin by HD cooling, a temperature regime that is never attained in our calculations (see, e.g., Nagakura & Omukai 2005; McGreer & Bryan 2008; Wolcott-Green & Haiman 2011; Nakauchi et al. 2014).

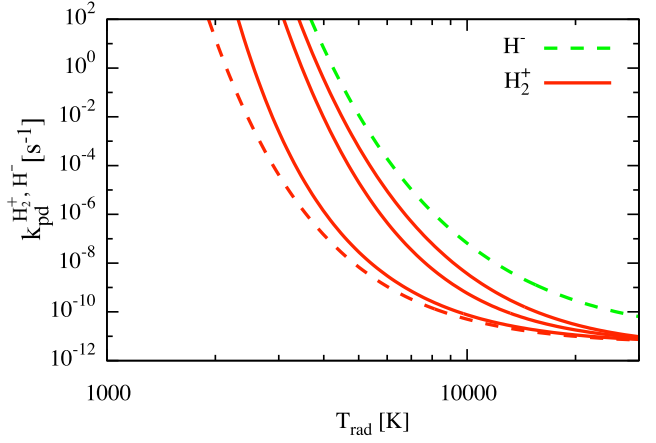


**Figure 1.** Photodissociation rate of  $\text{H}_2^+$  from the ground vibrational state (dashed red curve) and assuming LTE level populations with  $T_{\text{rad}} = 1000, 3000$  and  $8000$  K (solid red curves, bottom to top). The dashed green curve shows the  $\text{H}^-$  photodetachment rate. The radiation spectrum is a diluted black-body normalized as  $J_{21} = 1$ .

The processes involving  $\text{H}_2^+$  are the following. The vibrationally resolved reactions in our code are  $\text{H}_2^+$  formation by radiative association (reaction 3),  $\text{H}_2^+$  photodissociation (reaction 6),  $\text{H}_2^+$  dissociation by charge transfer (reaction 4), vibrational excitation/de-excitation by collision with  $\text{H}$  and vibrational de-excitation by spontaneous emission. We do not resolve rotational levels of  $\text{H}_2^+$ , because the dependence of the efficiency of  $\text{H}_2^+$  photodissociation on rotational levels is weaker than on vibrational levels (Dunn 1968; Babb 2014). In addition, complete rovibrational state-resolved data are not available in the literature. Note that  $\text{H}_2^+$  formation via  $\text{HeH}^+$  hardly affects the evolution of primordial clouds (see, however, GP98 or C11 for its consequences on the chemistry of the early Universe).

The state-resolved data adopted in our chemical network are the following. Babb (2014) provides rovibrationally resolved data for radiative association and  $\text{H}_2^+$  photodissociation, which are summed up with respect to rotational levels to obtain the vibrationally resolved rate coefficients. To obtain vibrationally resolved  $\text{H}_2^+$  photodissociation rate we assume rotational level population as explained in Appendix A. Fig. 1 shows the  $\text{H}_2^+$  photodissociation rates  $k_{\text{pd}}^{\text{H}_2^+}$  for a black-body radiation field and  $J_{21} = 1$ , obtained assuming (rovibrational) LTE population with  $T_{\text{rad}} = 1000, 3000$  and  $8000$  K, and all  $\text{H}_2^+$  in the ground state. Fig. 1 clearly shows that  $\text{H}_2^+$  becomes more easily photodissociated as the  $\text{H}_2^+$  vibrational state becomes more excited. Krstić’s database (Krstić et al. 2002; Krstić 2005; Krstić & Schultz 1999; Krstić et al. 2002; Krstić & Janev 2003) provides vibrationally resolved data for charge transfer and vibrational excitation/de-excitation by collision with  $\text{H}$ . The rovibrationally resolved de-excitation rates of  $\text{H}_2^+$  by spontaneous emission are taken from Posen et al. (1983). They are summed up with respect to rotational levels to obtain the vibrationally resolved rates. To see the dependence of the evolution of the clouds on the assumed  $\text{H}_2^+$  level population, in addition to the standard state-resolved runs (hereafter *non-LTE model*), we also perform runs using the (rovibrational) LTE  $\text{H}_2^+$  photodissociation rate (hereafter *LTE*

model) and runs using the  $\text{H}_2^+$  photodissociation rate for  $\text{H}_2^+$  in the (rovibrational) ground state (hereafter *ground-state model*).

We review here our treatment of  $\text{H}^-$  photodetachment and indirect  $\text{H}_2$  photodissociation (the so-called Solomon process). Fig. 1 shows the  $\text{H}^-$  photodetachment rate coefficient  $k_{\text{pd}}^{\text{H}^-}$  for a black-body radiation field normalized to  $J_{21} = 1$  as a function of  $T_{\text{rad}}$ . Here the cross section by John (1988) is used. As seen in Fig. 1, the  $\text{H}^-$  photodetachment is generally more effective than  $\text{H}_2^+$  photodissociation although the latter depends on the  $\text{H}_2^+$  level population. For the  $\text{H}_2$  photodissociation rate coefficient, we adopt the formula by Wolcott-Green et al. (2011),

$$k_{\text{pd}}^{\text{H}_2} = 1.4 \times 10^{-12} f_{\text{sh}} J_{21} \text{ s}^{-1}, \quad (9)$$

where  $f_{\text{sh}}$  is the self-shielding factor (for the explicit form, see eq. 10 of Wolcott-Green et al. 2011). For the radiation spectra considered in Fig. 5, Eq. (9) gives  $k_{\text{pd}}^{\text{H}_2} = 1.4 \times 10^{-12} \text{ s}^{-1}$  without self-shielding ( $f_{\text{sh}} = 1$ ). The fact that  $k_{\text{pd}}^{\text{H}_2^+}$  and  $k_{\text{pd}}^{\text{H}^-}$  are decreasing functions of  $T_{\text{rad}}$  can be understood as the photodissociation of  $\text{H}_2^+$  and the photodetachment of  $\text{H}^-$  are relatively more effective for softer spectra, compared to the photodissociation of  $\text{H}_2$ . Note that the exact form of  $f_{\text{sh}}$  is not settled in the literature (see, e.g., Draine & Bertoldi 1996; Wolcott-Green et al. 2011; Richings et al. 2014; Hartwig et al. 2015), which may introduce an uncertainty in the value of  $J_{21}^{\text{cr}}$  by a factor of a few, as pointed out in SOI14 and Glover (2015b). Similarly, evaluating  $k_{\text{pd}}^{\text{H}_2}$  with the intensity at a single frequency  $h\nu = 12.4 \text{ eV}$ , may introduce an uncertainty in the value of  $J_{21}^{\text{cr}}$  by a factor of a few if the spectrum changes substantially within the LW bands, as mentioned in SOI14. However, since the above uncertainties should not affect the conclusion of this paper, we leave these issues for future studies.

We updated the chemical network of SOI14, following Glover (2015a,b). We include dissociative tunneling of  $\text{H}_2$  to an unbound state (Martin et al. 1996) and H collisional ionization with H (Lenzuni et al. 1991; Gealy & van Zyl 1987) and He (Lenzuni et al. 1991; van Zyl et al. 1981). We replace the direct  $\text{H}_2$  collisional dissociation rate with the fit given in Martin et al. (1996).

### 2.3 Initial Conditions

Following Omukai et al. (2008) and SOI14, we take as initial conditions of the calculation the following values corresponding to the turnaround redshift  $z = 16$ :  $T_{\text{gas}} = 21 \text{ K}$ ,  $n_{\text{H}} = 4.5 \times 10^{-3} \text{ cm}^{-3}$ ,  $y(\text{e}) = 3.7 \times 10^{-4}$ ,  $y(\text{He}) = 8.3 \times 10^{-2}$ ,  $y(\text{H}_2) = 2 \times 10^{-6}$  and  $y(i) = 0$  for the other species. Note that the initial chemical composition hardly affects the thermal evolution of the clouds: at the beginning of the evolution well within the initial adiabatic contraction phase, most of pre-existing  $\text{H}_2$  is photodissociated under a strong LW radiation field with  $J_{21}$  around  $J_{21}^{\text{cr}}$ ;  $y(\text{e})$  settles to the value determined by the condition that the recombination time scale is about the same as the dynamical (free-fall) one; and the abundances of the other species reach the values in chemical equilibrium (Omukai 2001).

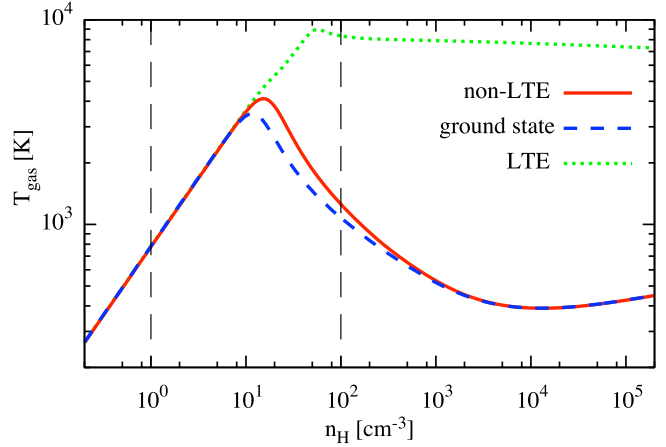


**Figure 2.** Temperature evolution in a collapsing primordial gas cloud irradiated by a diluted black-body radiation with  $T_{\text{rad}} = 6000 \text{ K}$  and  $J_{21} = 0.05$  as a function of the cloud density: non-LTE model (solid red), ground-state model (dashed blue) and LTE (dotted green). The vertical lines (long-dashed black) demarcate boundaries between the low, intermediate and high-density regimes.

## 3 RESULTS

In the following, we show how the temperature evolution of the cloud is modified by the assumed  $\text{H}_2^+$  vibrational level population. Then, we calculate the critical intensity of the radiation field  $J_{21}^{\text{cr}}$  as a function of the black-body temperature and assess the importance of  $\text{H}_2$  formation via the  $\text{H}_2^+$  channel on the evolution of the primordial clouds.

### 3.1 Thermal evolution of the cloud

The run of the temperature, chemical abundance and  $\text{H}_2^+$  level populations of a cloud irradiated by a black-body radiation field with  $T_{\text{rad}} = 6000 \text{ K}$  and  $J_{21} = 0.05$  as a function of the H number density are shown Figs. 2, 3 and 4, respectively. In Figs. 2 and 3 we also plot for comparison purposes the results for the ground-state and LTE models, along with the fiducial results for the non-LTE model. In Fig. 4, instead, we also plot the LTE populations with the temperature given by  $T_{\text{gas}}$  in the non-LTE model (i.e., the solid red curve in Fig.2) along with the results for the non-LTE model, because the difference in  $T_{\text{gas}}$  in the non-LTE and LTE models makes it difficult to extract the effect of non-LTE chemistry by directly comparing the populations in these models. The results for the LTE model agree well with those in SOI14, the differences being due to the updated chemical network. Below, we describe the time (or, equivalently, density) evolution of the cloud with particular attention to the  $\text{H}_2^+$  vibrational level population.

#### 3.1.1 Low-density Regime: $n_{\text{H}} \lesssim 1 \text{ cm}^{-3}$

In this density range, the temperature is still very low,  $T_{\text{gas}} \lesssim 10^3 \text{ K}$ , although it rises with density by adiabatic compression, as seen in Fig. 2. Thus, almost all  $\text{H}_2^+$  is in the ground vibrational state if LTE is assumed (Fig. 4). However, in the non-LTE model a finite amount of  $\text{H}_2^+$  is in higher vibrational levels because the  $\text{H}_2^+$  molecules tend to

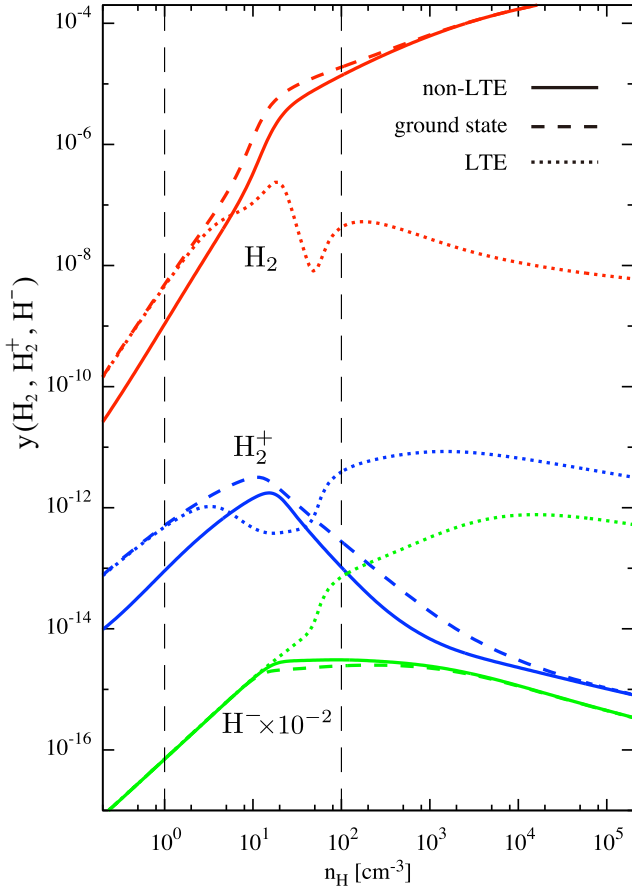


**Figure 3.** Abundances of  $\text{H}_2$  (red),  $\text{H}_2^+$  (blue) and  $\text{H}^-$  ( $\times 10^{-2}$ ; green) for the same cases as Fig. 2: non-LTE model (solid), ground-state model (dashed), and LTE (dotted) models.

be formed by radiative association in excited states (reaction 4; Ramaker & Peek (1976); Babb (2014)). This effect is more pronounced at low temperatures where the  $v = 15$  level is more populated than the  $v = 5$  and 10 levels. Note that not all the  $\text{H}_2^+$  settles to the ground state even though the collisional excitation/de-excitation rate is much smaller than the radiative de-excitation rate in this low-density regime. This is because not only radiative de-excitation, but also radiative association and  $\text{H}_2^+$  photodissociation contribute to the  $\text{H}_2^+$  level population. In the non-LTE model, since a fraction of  $\text{H}_2^+$  is in high vibrational levels, the larger  $\text{H}_2^+$  photodissociation reaction rate results in a smaller  $\text{H}_2^+$  abundance than in the LTE or ground-state models (Fig. 3). As a result, the amount of  $\text{H}_2$  formed is smaller in the non-LTE case. However, in this density range, the  $\text{H}_2$  abundance is very low,  $f_{\text{H}_2} \sim 10^{-9}$ , in all models and does not affect the thermal evolution.

### 3.1.2 Intermediate-density Regime: $n_{\text{H}} \sim 1 - 10^2 \text{ cm}^{-3}$

In this density regime, the evolutionary paths bifurcate into those of atomic and  $\text{H}_2$  cooling depending on the assumed level population (Fig. 2). As seen in Fig. 4, at high temperature ( $\sim 4000 \text{ K}$ ), in the LTE approximation the excited levels are somewhat populated around  $\sim 10 \text{ cm}^{-3}$ . However, in the non-LTE treatment only a smaller amount of  $\text{H}_2^+$  re-

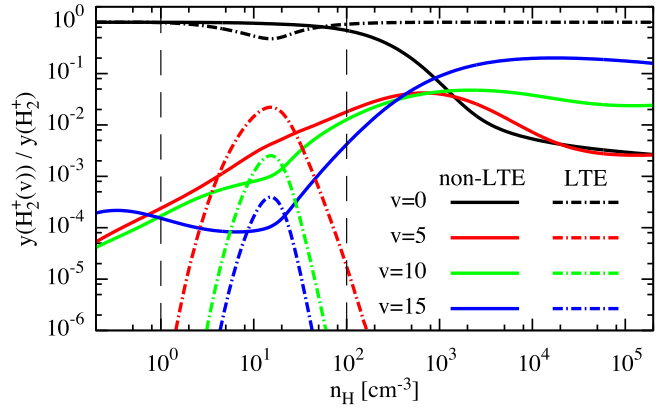


**Figure 4.** Populations of  $\text{H}_2^+$  in the  $v = 0, 5, 10,$  and  $15$  vibrational levels (black, red, green and blue, respectively) in the non-LTE model (solid) for the same case as Fig. 2. The LTE populations (dot dashed) with the temperature given by  $T_{\text{gas}}$  in the non-LTE model, i.e., the solid red curve in Fig. 2, are also plotted.

sides in excited states, because of the higher photodissociation rate from those levels. In LTE the fractional abundance of excited levels, and thus the  $\text{H}_2^+$  photodissociation rate are overestimated. This results in smaller amounts of both  $\text{H}_2^+$  and  $\text{H}_2$ , compared to the non-LTE model (Fig. 3). Due to the lower  $\text{H}_2$  fraction of the LTE case, the cloud collapses along the atomic cooling track, whereas in non-LTE it follows the molecular hydrogen cooling path (Fig. 2). Finally, in the ground-state model, the smaller  $\text{H}_2^+$  photodissociation rate and the consequent larger amount of  $\text{H}_2$  (Fig. 3) cause an earlier onset of  $\text{H}_2$  cooling relative to the non-LTE case (Fig. 2).

### 3.1.3 High-density regime: $n_{\text{H}} \gtrsim 10^2 \text{ cm}^{-3}$

The different evolutionary paths found in the previous regime are not modified at higher densities by the details of the various chemical processes. Considering the large temperature difference between LTE and the other models, it is not possible to distinguish between the effects of the level population and those related to the chemical abundances shown in Fig. 3. In this regime, unlike the LTE population, the excited levels are more populated than the ground state, as seen in Fig. 4. The reason is as follows: due to the high density, the  $\text{H}_2^+$  photodissociation is negligible compared to collisional processes, such as radiative association, charge transfer and collisional excitation/de-excitation. Since not only collisional excitation/de-excitation, but also radiative association and charge transfer continue to play important roles, the level population does not converge to the LTE value. This effect can be considered as a pumping mechanism that depletes the ground level and allows for the occupation of higher excited states.

## 3.2 The critical LW intensity $J_{21}^{\text{cr}}$

Fig. 5 shows the critical LW intensity  $J_{21}^{\text{cr}}$  for the black-body spectra with temperature  $T_{\text{rad}}$ . We find  $J_{21}^{\text{cr}}$  by using the bisection method, in which we examine whether the given  $J_{21}$  is high enough for the cloud to collapse along the atomic-cooling track by totally suppressing  $\text{H}_2$  cooling (for more

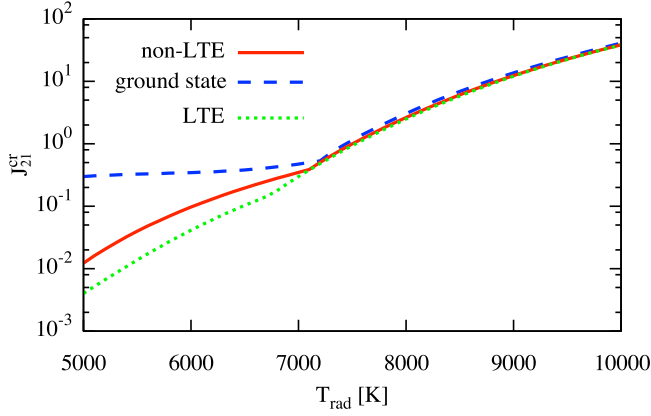


**Figure 5.** Critical intensity for the direct collapse  $J_{21}^{cr}$  as a function of the black-body temperature  $T_{rad}$  of the irradiation radiation. In addition to the value in the non-LTE model (solid red), those in the ground-state (dashed blue) and LTE (dotted green) models are plotted.

details, see, e.g., SOI14 and references therein). In addition to our fiducial result for the non-LTE model, those for the ground-state and LTE models are also plotted in Fig. 5 for comparison.

Two features in Fig. 5 should be noted. First, the slope of  $J_{21}^{cr}$  changes discontinuously around  $T_{rad} \sim 7000$  K, accompanying the shift of dominant  $H_2$ -formation reaction determining  $J_{21}^{cr}$  from the  $H_2^+$  channel ( $T_{rad} \lesssim 7000$  K) to the  $H^-$  channel ( $T_{rad} \gtrsim 7000$  K). We will discuss the condition for the  $H_2^+$  channel to be dominant in Sec. 3.3. Second, in the range  $T_{rad} \lesssim 7000$  K,  $J_{21}^{cr}$  depends on the assumed  $H_2^+$  vibrational populations. Therefore, it is necessary to take into account the non-LTE  $H_2^+$  level population to obtain  $J_{21}^{cr}$  correctly because the efficiency of the  $H_2^+$  channel, the dominant  $H_2$  formation channel in this range, is sensitive to its vibrational level population. Compared to the correct  $J_{21}^{cr}$  by the non-LTE modelling, those for the ground-state and LTE models are smaller or larger, respectively. This is because in the ground-state model (the LTE model), compared to the non-LTE model, the  $H_2^+$  photodissociation rate is lower (higher) around the density where the bifurcation into the two evolutionary paths occurs, and thus more (less)  $J_{21}$  is needed to suppress the  $H_2$  cooling.

On the other hand,  $J_{21}^{cr}$  for  $T_{rad} \gtrsim 7000$  K is insensitive to the  $H_2^+$  level population because the  $H^-$  channel rather than the  $H_2^+$  channel is important in this range to determine  $J_{21}^{cr}$ . Recall that typical high- $z$  galaxies have hard spectra corresponding to a black-body with  $T_{rad} \gtrsim 2 \times 10^4$  K (SOI14), as mentioned in Sec. 2.1. Thus, our adoption of the LTE  $H_2^+$  photodissociation rate in SOI14 to obtain  $J_{21}^{cr}$  for realistic spectra is justified. We plot  $J_{21}^{cr}$  only for  $T_{rad} < 10^4$  K in Fig. 5, because  $J_{21}^{cr}$  does not depend on the vibrational populations for  $T_{rad} > 10^4$  K. For  $J_{21}^{cr}$  in the range  $T_{rad} > 10^4$  K, we refer readers to, e.g., Fig. 3 of SOI14.

### 3.3 Condition for the $H_2^+$ -channel dominance

Here, we discuss the condition that the  $H_2^+$ -channel dominates over the  $H^-$  channel. We introduce  $J_{21}^{eq}$ , the threshold value of  $J_{21}$  above which the  $H_2^+$  channel is more effective in  $H_2$  formation than the  $H^-$  channel.

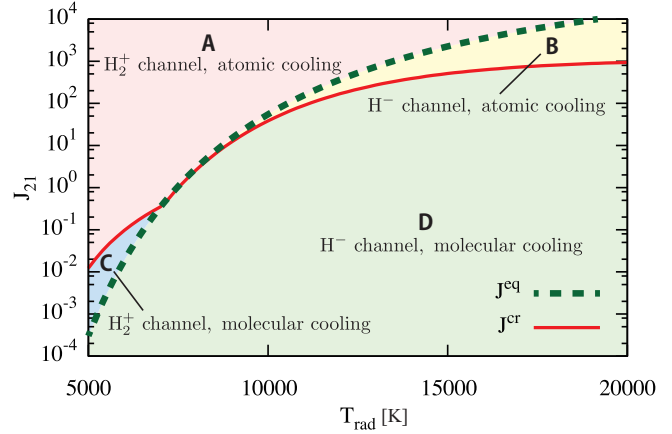


**Figure 6.** The threshold value  $J_{21}^{eq}$  (dashed green), given by Eq. (14), above which the  $H_2^+$  channel is more effective than the  $H^-$  channel at  $n_H = 10^2 \text{ cm}^{-3}$ . The critical intensity  $J_{21}^{cr}$  for the direct collapse shown in Fig. 5 (solid red) is overplotted. The explanation for the domains A-D is given in the text.

To begin with, we estimate the  $H_2$  formation rate via the  $H^-$  channel. The  $H^-$  fraction is determined by the balance between the radiative attachment (reaction 1), associative detachment (reaction 2) and photodetachment (reaction 5) as:

$$y(H^-) = \frac{k_{ra}^{H^-} y(e)}{k_{ad}^{H^-} + k_{pd}^{H^-}/n(H)}. \quad (10)$$

The  $H_2$  formation rate via the  $H^-$  channel is given by

$$\begin{aligned} \frac{dy_{H_2}}{dt} &= k_{ad}^{H^-} y(H^-) n(H) \\ &\simeq \frac{k_{ra}^{H^-} y(e) n(H)}{1 + k_{pd}^{H^-}/(n(H) k_{ad}^{H^-})}, \end{aligned} \quad (11)$$

where we have used Eq. (10) in the second line. Similarly, we estimate the  $H_2$  formation rate via the  $H_2^+$  channel. The  $H_2^+$  fraction is determined by the balance between radiative association (reaction 3), charge transfer (reaction 4) and photodissociation (reaction 6) as:

$$y(H_2^+) = \frac{k_{ra}^{H_2^+} y(H^+)}{k_{ct}^{H_2^+} + k_{pd}^{H_2^+}/n(H)}. \quad (12)$$

The  $H_2$  formation rate via the  $H_2^+$  channel, i.e., the charge transfer rate, is given by

$$\begin{aligned} \frac{dy_{H_2}}{dt} &= k_{ct}^{H_2^+} y(H_2^+) n(H) \\ &\simeq \frac{k_{ra}^{H_2^+} y(H^+) n(H)}{1 + k_{pd}^{H_2^+}/(n(H) k_{ct}^{H_2^+})}, \end{aligned} \quad (13)$$

where we have used Eq. (12) in the second line. By equating Eqs. (11) and (13), we obtain

$$J_{21}^{eq} \simeq \left( \frac{k_{ra}^{H^-}}{k_{ra}^{H_2^+}} - 1 \right) \frac{k_{ad}^{H^-} n_H}{k_{pd}^{H^-} |_{J_{21}=1}}, \quad (14)$$

where we have used  $k_{pd}^{H^-} = k_{pd}^{H^-} |_{J_{21}=1} \times J_{21}$ ,  $n(H) \simeq n_H$

and  $y(e) \simeq y(\text{H}^+)$  and neglected  $k_{\text{pd}}^{\text{H}_2^+}$  for simplicity. The effect of  $\text{H}_2^+$  photodissociation would substantially change the expression given by Eq. (14) if the LTE rate was used. However, the actual rate of  $\text{H}_2^+$  photodissociation just before the atomic- and  $\text{H}_2$ -cooling tracks bifurcate is lower than the LTE one, as shown in Sec. 3.1.2. Thus, the correction due to  $\text{H}_2^+$  photodissociation makes  $J_{21}^{\text{eq}}$  given by Eq. (14) larger at most by a factor of a few and can be neglected in the order-of-magnitude estimate here.

To evaluate  $J_{21}^{\text{eq}}$ , we consider the physical condition of the gas just before the atomic- and  $\text{H}_2$ -cooling tracks bifurcate (see, e.g., Omukai (2001) or SOI14) and take  $T_{\text{gas}} = 8000 \text{ K}$  and  $n_{\text{H}} = 10^2 \text{ cm}^{-3}$ . The density  $n_{\text{H}}$  at bifurcation depends on the spectra and it is closer to  $10^2 \text{ cm}^{-3}$  for soft spectra with  $T_{\text{rad}} \lesssim 10^4 \text{ K}$ , which is of our interest in this paper, although it is about  $10^3 \text{ cm}^{-3}$  for  $T_{\text{rad}} \sim 10^5 \text{ K}$ . The reaction rate coefficients at 8000 K are given by  $k_{\text{ra}}^{\text{H}^-} \approx 6 \times 10^{-15} \text{ cm}^3 \text{ s}^{-1}$ ,  $k_{\text{ad}}^{\text{H}^-} \approx 9 \times 10^{-10} \text{ cm}^3 \text{ s}^{-1}$  and  $k_{\text{ra}}^{\text{H}_2^+} \simeq 1.5 \times 10^{-16} \text{ cm}^3 \text{ s}^{-1}$  (GP98) and the  $\text{H}^-$  photodetachment rate is given by Fig. 1. By substituting the above reaction rate coefficients and photodetachment rate into Eq. (14), we obtain  $J_{21}^{\text{eq}}$ , as shown in Fig. 6. Also shown is  $J_{21}^{\text{cr}}$  obtained in Sec. 3.2 for comparison. Depending on the value of  $J_{21}$  relative to  $J_{21}^{\text{cr}}$  and  $J_{21}^{\text{eq}}$ , the way in which a cloud evolves falls within one of the following four cases (Fig. 6):

A:  $J_{21} > J_{21}^{\text{cr}}$  and  $J_{21} > J_{21}^{\text{eq}}$ . The cloud collapses along the atomic-cooling track, since  $\text{H}_2$ , formed mainly via the  $\text{H}_2^+$  channel, is not enough to cool the gas.

B:  $J_{21} > J_{21}^{\text{cr}}$  and  $J_{21} < J_{21}^{\text{eq}}$ . The cloud collapses along the atomic-cooling track, since  $\text{H}_2$ , formed mainly via the  $\text{H}^-$  channel, is not enough to cool the gas.

C:  $J_{21} < J_{21}^{\text{cr}}$  and  $J_{21} > J_{21}^{\text{eq}}$ . The cloud collapses along the  $\text{H}_2$ -cooling track due to  $\text{H}_2$  formation mainly via the  $\text{H}_2^+$  channel.

D:  $J_{21} < J_{21}^{\text{cr}}$  and  $J_{21} < J_{21}^{\text{eq}}$ . The cloud collapses along the  $\text{H}_2$ -cooling track due to  $\text{H}_2$  formation mainly via the  $\text{H}^-$  channel.

In the soft-spectrum regime of  $T_{\text{rad}} \lesssim 7000 \text{ K}$ , where  $J_{21}^{\text{eq}} \lesssim J_{21}^{\text{cr}}$ , the cases A, C, and D can be realized depending on  $J_{21}$ . In the case C, in particular, while the  $\text{H}^-$  channel is blocked by radiation, sufficient  $\text{H}_2$  for cooling can still form via the  $\text{H}_2^+$  channel. In this case, the proper account of the  $\text{H}_2^+$  level population is indispensable since the  $\text{H}_2$  formation rate via the  $\text{H}_2^+$  channel is sensitive to its level population, as shown by the example in Sec. 3.1. On the other hand, in the hard-spectrum regime of  $T_{\text{rad}} \gtrsim 7000 \text{ K}$ , where  $J_{21}^{\text{cr}} \lesssim J_{21}^{\text{eq}}$ , the cases A, B and D are allowed: there is no range of  $J_{21}$  satisfying  $J_{21}^{\text{eq}} < J_{21} < J_{21}^{\text{cr}}$ . Namely, radiation fields strong enough to block the  $\text{H}^-$  channel always exceed the critical intensity to totally suppress  $\text{H}_2$  formation by  $\text{H}_2$  photodissociation. This means that the  $\text{H}_2$ -cooling track cannot be realized by the  $\text{H}_2^+$  channel for  $T_{\text{rad}} \gtrsim 7000 \text{ K}$ .

## 4 DISCUSSION AND CONCLUSIONS

We have computed the thermal and chemical evolution of primordial gas clouds resolving the vibrational levels of  $\text{H}_2^+$ , which enables us to properly implement  $\text{H}_2$  formation via the  $\text{H}_2^+$  channel. The efficiency of  $\text{H}_2^+$  photodissociation, which

suppresses the  $\text{H}_2^+$  channel by destroying the intermediate product  $\text{H}_2^+$ , is sensitive to the level population of the molecular ion. We have found that  $\text{H}_2$  formation via the  $\text{H}_2^+$  channel becomes more effective in the non-LTE model than in LTE because more  $\text{H}_2^+$  is in the ground state and thus its photodissociation rate is smaller.

As to the effects of the background radiation, we have found that  $\text{H}_2$  formation via the  $\text{H}_2^+$  channel becomes important in clouds irradiated by strong radiation fields with soft spectra characterised by  $T_{\text{rad}} \lesssim 7000 \text{ K}$ . In this case, the cloud thermal evolution is strongly affected by the  $\text{H}_2^+$  level population, indicating the importance of non-LTE treatment of the  $\text{H}_2^+$  vibrational levels. On the other hand, under radiation fields with harder spectra and  $T_{\text{rad}} \gtrsim 7000 \text{ K}$ , the  $\text{H}_2^+$  channel always falls short of the  $\text{H}^-$  channel in producing  $\text{H}_2$  molecules.

We have derived the critical radiation intensity  $J_{21}^{\text{cr}}$  for the formation of supermassive stars by direct collapse and examined its dependence on the assumed  $\text{H}_2^+$  level population. For soft spectra with  $T_{\text{rad}} \lesssim 7000 \text{ K}$ , the critical intensity  $J_{21}^{\text{cr}}$  is under(over)-estimated if the level population is assumed to be in LTE (if all the  $\text{H}_2^+$  is assumed to be in the ground state). On the other hand, the value of  $J_{21}^{\text{cr}}$  is independent of the assumed  $\text{H}_2^+$  level population for harder spectra with  $T_{\text{rad}} \gtrsim 7000 \text{ K}$ . Therefore, since typical high-redshift radiation sources, i.e., young and/or metal-poor galaxies, have rather hard spectra corresponding to black-bodies with  $T_{\text{rad}} \gtrsim 2 \times 10^4 \text{ K}$  (SOI14), the LTE approximation adopted in SOI14 in determining  $J_{21}^{\text{cr}}$  for realistic spectra is justified.

We note that primordial gas clouds may be exposed to much softer radiation fields. For example, galaxies with extremely strong Ly- $\alpha$  emission can be regarded as characterised by very soft spectra. Since the energy of Ly- $\alpha$  photons ( $h\nu = 10.2 \text{ eV}$ ) is below the lower limit of the Lyman-Werner bands ( $h\nu = 11.2 - 13.6 \text{ eV}$ ), such emission would only destroy  $\text{H}^-$  leaving  $\text{H}_2$  unaffected. Also, since the initial mass function in high-redshift galaxies is poorly constrained, the infrared/optical cosmic background radiation originating from these sources can be soft with temperature  $T_{\text{rad}} \sim 6000 \text{ K}$ , corresponding to the typical stellar mass  $\sim 0.7 M_{\odot}$ , as considered in Wolcott-Green & Haiman (2012).

In non-standard cosmology primordial density fluctuations are expected to be enhanced at small scales, so that the first stellar objects can form at very early times with  $z \gtrsim 100$ , as considered in Hirano et al. (2015). Under the strong and very soft CMB radiation at that time ( $T_{\text{rad}} \gtrsim 300 \text{ K}$ ),  $\text{H}_2$  formation via the  $\text{H}_2^+$  channel can be the dominant path with the  $\text{H}^-$  channel blocked by radiation processes (including non-thermal photons that play an additional role in enhancing  $\text{H}^-$  photodetachment; Coppola et al. 2013).

As a last example, let us consider the case where direct collapse via the atomic-cooling track is realized. In such a case, the growing protostar results in a very extended structure with radius  $R \simeq 30 \text{ AU}$  (“super-giant” protostar) and low effective temperature  $T_{\text{rad}} \simeq 5000 \text{ K}$  (Hosokawa et al. 2012, 2013). In studying the physical conditions in the region around the super-giant protostar, the non-LTE  $\text{H}_2^+$  level population must be taken into account.

In this paper, the collapse of primordial gas clouds has been calculated by resolving the  $\text{H}_2^+$  vibrational levels, to

our knowledge, for the first time. However, neither  $\text{H}_2^+$  rotational levels nor  $\text{H}_2$  rovibrational levels have been explicitly included. Although the  $\text{H}_2^+$  rotationally-resolved kinetics is probably not important, the  $\text{H}_2$  rovibrationally-resolved kinetics may have considerable effects. The  $\text{H}_2$  rovibrational level population affects critical processes in the evolution of the primordial gas, such as photodissociation, collisional dissociation, and cooling by molecular hydrogen. We plan to include the full level-resolved kinetics of  $\text{H}_2$  and  $\text{H}_2^+$  in future studies.

KS would like to thank D. Nakauchi, H. Yajima and K. Toma for fruitful discussions and valuable comments. KS would also like to thank Savino Longo and University of Bari for hospitality and support during his visit to University of Bari. This work is supported in part by MEXT/JSPS KAKENHI Grant Number 15J03873 (KS) and 25287040 (KO). The authors acknowledge the discussions within the international team #272 lead by C. M. Coppola “EUROPA - Early Universe: Research on Plasma Astrochemistry” at ISSI (International Space Science Institute) in Bern.

## REFERENCES

- Agarwal, B., & Khochfar, S. 2015, *MNRAS*, 446, 160
- Agarwal, B., Khochfar, S., Johnson, J. L., et al. 2012, *MNRAS*, 425, 2854
- Anninos, P., Zhang, Y., Abel, T., & Norman, M. L. 1997, *New Astron.*, 2, 209
- Babb, J. F. 2015, *ApJS*, 216, 21
- Becerra, F., Greif, T. H., Springel, V., & Hernquist, L. E. 2015, *MNRAS*, 446, 2380
- Bromm, V., & Loeb, A. 2003, *ApJ*, 596, 34
- Choi, J.-H., Shlosman, I., & Begelman, M. C. 2015, *MNRAS*, 450, 4411
- Coppola, C. M., Longo, S., Capitelli, M., Palla, F., & Galli, D. 2011, *ApJS*, 193, 7 (C11)
- Coppola, C. M., Galli, D., Palla, F., Longo, S., & Chluba, J., 2013, *MNRAS*, 434, 1, 114
- Dijkstra, M., Ferrara, A., & Mesinger, A. 2014, *MNRAS*, 442, 2036
- Dijkstra, M., Haiman, Z., Mesinger, A., & Wyithe, J. S. B. 2008, *MNRAS*, 391, 1961
- Draine, B. T., & Bertoldi, F. 1996, *ApJ*, 468, 269
- Dunn, G. H. 1968, *Physical Review*, 172, 1
- Fan, X., Narayanan, V. K., Lupton, R. H., et al. 2001, *AJ*, 122, 2833
- Galli, D., & Palla, F. 1998, *A&A*, 335, 403 (GP98)
- Gealy, M. W., & van Zyl, B. 1987, *Phys. Rev. A*, 36, 3100
- Glover, S. 2015a, *MNRAS*, 451, 2082
- Glover, S. C. O. 2015b, *MNRAS*, 453, 2901
- Glover, S. C. O., & Abel, T. 2008, *MNRAS*, 388, 1627
- Hartwig, T., Glover, S. C. O., Klessen, R. S., Latif, M. A., & Volonteri, M. 2015, *MNRAS*, 452, 1233
- Hirano, S., Zhu, N., Yoshida, N., Spergel, D., & Yorke, H. W. 2015, *ArXiv e-prints*, arXiv:1504.05186
- Hirata, C. M., & Padmanabhan, N. 2006, *MNRAS*, 372, 1175
- Hosokawa, T., Omukai, K., & Yorke, H. W. 2012, *ApJ*, 756, 93
- Hosokawa, T., Omukai, K., Yoshida, N., & Yorke, H. W. 2011, *Science*, 334, 1250
- Hosokawa, T., Yorke, H. W., Inayoshi, K., Omukai, K., & Yoshida, N. 2013, *ApJ*, 778, 178
- Inayoshi, K., Omukai, K., & Tasker, E. 2014, *MNRAS*, 445, L109
- Inayoshi, K., & Tanaka, T. L. 2015, *MNRAS*, 450, 4350
- John, T. L. 1988, *A&A*, 193, 189
- Krstić, P. S. 2005, *Nuclear Instruments and Methods in Physics Research B*, 241, 58
- Krstić, P. S., & Janev, R. K. 2003, *Phys. Rev. A*, 67, 022708
- Krstic, P. S., & Schultz, D. R. 1999, *Journal of Physics B Atomic Molecular Physics*, 32, 2415
- Krstić, P. S., Schultz, D. R., & Janev, R. K. 2002, *Physica Scripta Volume T*, 96, 61
- Larson, R. B. 1969, *MNRAS*, 145, 271
- Latif, M. A., Bovino, S., Van Borm, C., et al. 2014, *MNRAS*, 443, 1979
- Lenzuni, P., Chernoff, D. F., & Salpeter, E. E. 1991, *ApJS*, 76, 759
- Longo, S., Coppola, C. M., Galli, D., Palla, F. & Capitelli, M., 2011, *Rend. Fis. Acc. Lincei*, 22, 119
- Martin, P. G., Schwarz, D. H., & Mandy, M. E. 1996, *ApJ*, 461, 265
- McGreer, I. D., & Bryan, G. L. 2008, *ApJ*, 685, 8
- Mihajlov, A. A., Ignjatović, L. M., Sakan, N. M., & Dimitrijević, M. S. 2007, *A&A*, 469, 749
- Mortlock, D. J., Warren, S. J., Venemans, B. P., et al. 2011, *Nature*, 474, 616
- Nagakura, T., & Omukai, K. 2005, *MNRAS*, 364, 1378
- Nakauchi, D., Inayoshi, K., & Omukai, K. 2014, *MNRAS*, 442, 2667
- Omukai, K. 2001, *ApJ*, 546, 635
- Omukai, K., Schneider, R., & Haiman, Z. 2008, *ApJ*, 686, 801
- Penston, M. V. 1969, *MNRAS*, 144, 425
- Posen, A. G., Dalgarno, A., & Peek, J. M. 1983, *Atomic Data and Nuclear Data Tables*, 28, 265
- Ramaker, D. E., & Peek, J. M. 1976, *Phys. Rev. A*, 13, 58
- Regan, J. A., & Haehnelt, M. G. 2009a, *MNRAS*, 393, 858
- , 2009b, *MNRAS*, 396, 343
- Regan, J. A., Johansson, P. H., & Haehnelt, M. G. 2014a, *MNRAS*, 439, 1160
- Regan, J. A., Johansson, P. H., & Wise, J. H. 2014b, *ApJ*, 795, 137
- Richings, A. J., Schaye, J., & Oppenheimer, B. D. 2014, *MNRAS*, 442, 2780
- Sakurai, Y., Hosokawa, T., Yoshida, N., & Yorke, H. W. 2015, *MNRAS*, 452, 755
- Shang, C., Bryan, G. L., & Haiman, Z. 2010, *MNRAS*, 402, 1249
- Shapiro, S. L., & Teukolsky, S. A. 1983, *Black holes, white dwarfs, and neutron stars: The physics of compact objects* (New York: Wiley)
- Shlosman, I., Choi, J.-H., Begelman, M. C., & Nagamine, K. 2015, arXiv:1508.05098v1
- Stancil, P. C. 1994, *ApJ*, 430, 360
- Sugimura, K., Omukai, K., Inoue, A. K., 2014, *MNRAS*, 445, 1, 544 (SOI14)
- van Zyl, B., Le, T. Q., & Amme, R. C. 1981, *J. Chem. Phys.*, 74, 314
- Venemans, B. P., Findlay, J. R., Sutherland, W. J., et al.



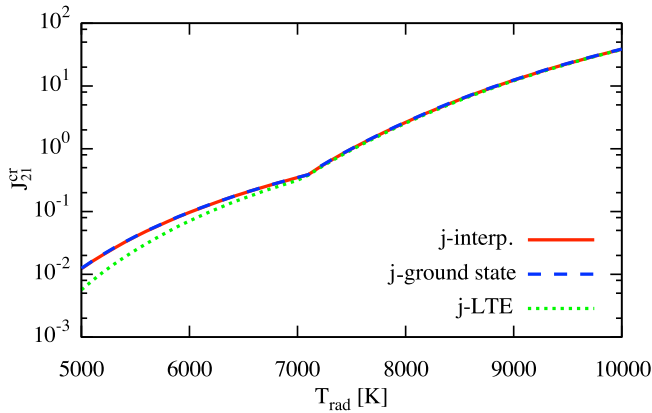


**Figure A1.** Same as Fig. 5, but for three different assumptions on the  $\text{H}_2^+$  rotational level population: (i) model using the interpolation formula by Glover (2015a), (ii) model where all the  $\text{H}_2^+$  in each vibrational level is in its rotational ground state. and (iii) model assuming the rotational LTE. Note that the  $\text{H}_2^+$  vibrational levels are resolved in all the cases.

2013, ApJ, 779, 24

Wolcott-Green, J., & Haiman, Z. 2011, MNRAS, 412, 2603  
—, 2012, MNRAS, 425, L51

Wolcott-Green, J., Haiman, Z., & Bryan, G. L. 2011, MNRAS, 418, 838

Wu, X.-B., Wang, F., Fan, X., et al. 2015, Nature, 518, 512

Yahil, A. 1983, ApJ, 265, 1047

Yoshida, N., Omukai, K., & Hernquist, L. 2008, Science, 321, 669

## APPENDIX A: $\text{H}_2^+$ ROTATIONAL LEVEL POPULATION

Here, we describe our treatment of the  $\text{H}_2^+$  rotational level populations. Since comprehensive rotational-state-resolved data is not available in the literature, we use the interpolation formula by Glover (2015a). Specifically, we calculate the  $\text{H}_2^+$  photodissociation rate from each vibrational level by the formula  $k = k_{\text{LTE}} (k_{n \rightarrow 0} / k_{\text{LTE}})^\alpha$ , where  $k_{n \rightarrow 0}$  and  $k_{\text{LTE}}$  are the rates for the ground rotational state and the LTE rotational level population, respectively,  $\alpha = (1 + n_{\text{H}} / n_{\text{cr}})^{-1}$  and  $n_{\text{cr}}$  is the critical density for the LTE populations, which is  $\sim 10^3 \text{ cm}^{-3}$  for  $T_{\text{gas}} = 8000 \text{ K}$  (Glover 2015a).

To estimate the error in our modeling of the  $\text{H}_2^+$  rotational level population, we compare the critical intensity  $J_{21}^{\text{cr}}$  obtained with three different modeling of rotational level population: (i) the fiducial model based on Glover (2015a) (*j*-interp. model); (ii) the model assuming that all the  $\text{H}_2^+$  in each vibrational level resides in the ground rotational state (*j*-ground state model); and (iii) the model assuming the LTE rotational level population in each vibrational level (*j*-LTE model). Fig. A1 shows that the values of  $J_{21}^{\text{cr}}$  in the *j*-interp. and *j*-ground state models are almost identical while in the *j*-LTE model it is slightly smaller. This difference is, however, much smaller than that among the vibrationally non-LTE and LTE models shown in Fig. 5, indicating that the cloud thermal evolution does not depend so much on rotational level population as the vibrational level population.